Three-dimensional dynamic analysis for bridge-vehicle interaction with roadway roughness

Kim, Chul-Woo

Kawatani, Mitsuo

Kim, Ki Bong

(Citation)
Computers & Structures,83(19-20):1627-1645

(Issue Date)
2005-07

(Resource Type)
journal article

(Version)
Accepted Manuscript

(URL)
https://hdl.handle.net/20.500.14094/90000473

Three-dimensional dynamic analysis for bridge-vehicle interaction with roadway roughness

Chul Woo Kim[1,*], Mitsuo Kawatani[1] , Ki Bong Kim[2]

[1]*Department of Civil Engineering, Kobe University, 1-1 Rokkodai, Nada, Kobe 657-8501, Japan*

[2]*Department of Civil Engineering, Chung-Ang University, 72-1 Neri, Dedug, Ansung 456-756, Korea*

Abstract

A three-dimensional means of analysis is proposed for the bridge-vehicle interaction to investigate the dynamic responses of a steel girder bridge and vehicles. The governing equations of motion for a three-dimensional bridge-vehicle interaction system taking the roadway surface into account are derived using the Lagrange equation of motion while the coupled bridge-vehicle interaction system is solved using Newmark's β method. A cargo truck, dump truck and steel girder bridge are considered numerical models and measured roadway roughness profiles are used for analyses. The analytical dynamic wheel loads and acceleration responses of the heavy vehicles and responses of the bridge are compared with data from field tests to verify the validity of the proposed procedure. The correlation between the analytical and experimental results is satisfactory.

Keywords: bridge-vehicle interaction; dynamic wheel load; field test; three-dimensional dynamic analysis; traffic-induced vibration of bridge.

1. Introduction

The problem of vibration in bridge structures due to moving vehicle loads has been a topic of interest for over a century. One of the major external dynamic forces acting on bridges, especially those of short and medium span, is the moving vehicle load and effects, which vary over time, have been examined in terms of impact factors. The impact factor has therefore been one of the major topics in bridge dynamics [1, 2] since the mid nineteenth century. It is widely known that the dynamic responses of bridges depend on the vehicle type, speed, roughness of the pavement, bridge type, etc. (e.g. Refs. [2-11]), although the bridge design codes define the

* Corresponding author.
Department of Civil Engineering, Kobe University, 1-1 Rokkodai, Nada, Kobe 657-8501, Japan.
Phone: +81-78-803-6383; FAX: +81-78-803-6069.
E-mail addresses: cwkim@kobe-u.ac.jp (C.W. Kim), m-kawa@kobe-u.ac.jp (M. Kawatani), kbkim@cau.ac.kr(K.B. Kim).

impact factor as a function of the bridge span length. Investigations into bridge-vehicle interaction have been carried out by many researchers and several topics relating to this area have already been fully reviewed by Cantieni in a recent article [2].

There are two means of investigating the complicated bridge-vehicle interaction problem: namely experimental and analytical approaches. The experimental method requires considerable time, facilities and cost while the analytical approach represents an economical way to examine the bridge-vehicle interaction provided the validity of this method be verified.

One of the most common analytical approaches to examine the problems concerning bridge-vehicle interaction has been a method using one- or two-dimensional models of bridges and vehicles [7, 9-10, 12-15]. The two-dimensional system can provide good analytical results for investigating the dynamic responses of whole bridge structures induced by moving vehicles on uneven roadways [9-10, 13, 15]. The three-dimensional bridge-vehicle interaction system is usually adopted to simulate the responses of local bridge components such as deck slabs and cross beams [16], and to investigate bridge responses induced by vehicles with paths that do not follow the center line of the bridge. A few three-dimensional analytical models for the bridge-vehicle interaction system thus have been developed (e.g. references [11, 17-18]). However, most of the previous works to date have focused on bridge responses, although forces producing bridge stresses due to moving vehicular loadings are the results of the vehicle's dead weights and the force of interaction between vehicle-pavement-bridge. Furthermore, there has been relatively little verification of analytical results irrespective of their importance in bridge dynamics, even the case of considering dynamic vehicular loads.

The major goal of this study is to develop a procedure for determining the dynamic wheel loads of vehicles as well as the bridge responses thereto, and to verify the validity of the analytical procedure. To meet the needs of this study, the governing equations of the bridge-vehicle interaction system are derived using Lagrange's formulation, and the numerical model for the traffic-induced vibration of bridges makes use of the finite element method for modal analysis. Newmark's β method [19] is applied to solve the derived system governing motion equations. The approach is then validated through comparison with field test data.

2. Idealizations and assumptions

2.1. Idealization of vehicle system

The two-axle Ford cargo truck (one front and rear axle) [20-22] is idealized as a vehicle model of offering seven-degrees-of-freedom (7DOF) (see Fig. 1(a)). The three-axle Isuzu dump truck (one front and two rear axles) [16, 22] meanwhile is idealized as a vehicle model with eight-degrees-of-freedom (8DOF) (see Fig. 1(b)). The vehicle body itself is considered to be rigid and supported by a set of linear springs and dashpots attached to each axle.

In Fig.1, Z_{11}, Z_{12}, Z_{22}, θ_{x11}, θ_{x12}, θ_{x22}, θ_{y11} and θ_{y22} refer to the bounce of vehicle body, the parallel hop of front and rear axle respectively, the rolling of vehicle body, the axle tramp of the front and rear axles, the pitching of vehicle body and the axle windup motion of the rear axle of the vehicle model, respectively. m_{v11}, m_{v12} and m_{v22}, respectively, indicate the concentrated mass of the vehicle body, front and rear axles. K_{vmku} and C_{vmku} are the spring constant and damping coefficient of a vehicle; the subscript *k* is the index to indicate the vehicle body and axle (*k*=1, 2 indicating the vehicle body and axle, respectively), subscript *m* is the index for the axle/tire positions (if *k*=1 then *m*=1, 2 indicating front and rear axle, respectively; if *k*=2 then *m*=1, 2, 3 indicating the tire at the front-axle, front and rear tires of the rear axle, respectively) and subscript *u* is the index for indicating the left and right sides of a vehicle (*u*=1, 2 indicating left and right sides, respectively). The sign is taken to be positive if the deformation occurs in a downward direction, pitching occurs from the rear to the front axle and rolling is generated from the right to left side.

2.2. Idealization of bridge system

The finite element (FE) method and modal analysis are adopted as the tools for idealizing bridges for dynamic response analysis. The lumped mass system and Rayleigh damping [23] are adopted to form mass and damping matrices of the bridge model, respectively.

Two types of finite elements are adopted to idealize members of the bridge super-structure. Beam elements with six-degrees-of-freedom at each node are used to idealize girders, cross beams and guard rails of a bridge. Decks are idealized as a flat plate element with four nodes [24]. To improve the efficiency of calculation, a process known as Guyan reduction is performed [25].

2.3. Idealization of bridge-vehicle interaction system

Figure 2 is the idealized bridge-vehicle interaction system with the pavement surface in a deformed state [17]. Z_{0mu} denotes the relative displacement defined by the difference between the displacement of bridge and surface roughness at the contact point of each tire. The longitudinal position of the tire location x_{mu} is relative to the bridge entry. The pavement roughness of the bridge at a tire location is denoted by Z_{rmu}. $w(t,x_{mu})$ is the elastic deformation of the bridge at a time *t* and a location x_{mu} while the subscripts *m* and *u* are the same indices explained in Section 2.1.

The assumptions considered in this study are: 1) the bridge follows Hooke's law, Navier's hypothesis, Saint-Venant's principle and small-deflection theory, 2) the ground acceleration and support settlement of the bridge are not taken into account, 3) the bridge is initially at rest before the vehicle enters the span, 4) the vehicle speed and path are constant, 5) the vehicle body is treated as a rigid body: the elastic behavior of the body is not

considered and 6) the suspension springs are assumed to be linearly elastic and the damping of the suspension system is considered to be viscous.

3. Equations of motion of bridge-vehicle interaction system

The method known as the Lagrange equation of motion has been known as one of the most popular methods to formulate a dynamic system since the French mathematician Lagrange discovered a relationship providing a genuinely powerful and flexible method to formulate equations of motion for any dynamical system. Therefore, governing equations of the bridge-vehicle interaction system are derived from the energy method using the Lagrange equation of motion as shown in Eq. (1) [7, 26].

$$\frac{d}{dt}\left(\frac{\partial T}{\partial \dot{q}_i}\right) - \frac{\partial T}{\partial q_i} + \frac{\partial V}{\partial q_i} + \frac{\partial U_d}{\partial \dot{q}_i} = 0 \tag{1}$$

where, T is kinetic energy of the system; V, potential energy of the system; U_d, dissipation energy of the system; q_i, the ith generalized co-ordinate.

The kinetic energy, potential energy including strain and dissipation energies of the bridge-vehicle interaction system are expressed in a set of generalized coordinates as follows:

$$T = \frac{1}{2}\dot{\mathbf{D}}^T\mathbf{M}_b\dot{\mathbf{D}} + \frac{1}{2}\left(m_{v11}\dot{Z}_{11}{}^2 + J_{y11}\dot{\theta}_{y11}{}^2 + J_{x11}\dot{\theta}_{x11}{}^2 + J_{y22}\dot{\theta}_{y22}{}^2 + m_{v12}\dot{Z}_{12}{}^2 + m_{v22}\dot{Z}_{22}{}^2 + J_{x12}\dot{\theta}_{x12}{}^2 + J_{x22}\dot{\theta}_{x22}{}^2\right) \tag{2}$$

$$V = \frac{1}{2}\mathbf{D}^T\mathbf{K}_b\mathbf{D} + \frac{1}{2}\sum_{m=1}^{3}\sum_{u=1}^{2}\left[K_{vm1u}R_{m1u}{}^2 + K_{vm2u}\left(R_{m2u} - Z_{0mu}\right)^2 + 2\cdot W_{mu}Z_{0mu}\right] \tag{3}$$

$$U_d = \frac{1}{2}\dot{\mathbf{D}}^T\mathbf{C}_b\dot{\mathbf{D}} + \frac{1}{2}\sum_{m=1}^{3}\sum_{u=1}^{2}\left[C_{vm1u}\dot{R}_{m1u}{}^2 + C_{vm2u}\left(\dot{R}_{m2u} - \dot{Z}_{0mu}\right)^2\right] \tag{4}$$

where

$$Z_{0mu} = w(t, x_{mu}) - Z_{rmu} \tag{5}$$

$$R_{mku} = \begin{cases} Z_{11} - (-1)^m\lambda_{xm}\theta_{y11} - (-1)^u\lambda_{y1}\theta_{x11} - Z_{m2} + (-1)^u\lambda_{y(m+1)}\theta_{xm2} & m=1,\ 2;\ k=1;\ u=1,\ 2 \\ Z_{12} - (-1)^u\lambda_{y2}\theta_{x12} & m=1;\quad k=2;\ u=1,\ 2 \\ Z_{22} + (-1)^m\lambda_{x3}\theta_{y2} - (-1)^u\lambda_{y3}\theta_{x22} & m=2,\ 3;\ k=2;\ u=1,\ 2 \\ 0 & \textit{otherwise} \end{cases} \tag{6}$$

$$W_{mu} = \begin{cases} \frac{1}{2} g\left[(1-\frac{\lambda_{x1}}{\lambda_x}) m_{v11} + m_{v12} \right] & m = 1; \quad u = 1, \ 2 \\ \frac{1}{4} g\left[(1-\frac{\lambda_{x2}}{\lambda_x}) m_{v11} + m_{v22} \right] & m = 2, \ 3; \ u = 1, \ 2 \\ 0 & otherwise \end{cases} \tag{7}$$

The superscript dot denotes the differential in terms of time. J in Eq. (2) and g in Eq. (7) indicate the mass moment of inertia of the vehicle and its gravity, respectively. In Eqs. (2)-(4), $\mathbf{D}$ and $\dot{\mathbf{D}}$ indicate the displacement and velocity vectors of the bridge, respectively; $\mathbf{M}_b$ and $\mathbf{K}_b$ respectively indicate the reduced mass and stiffness matrices [25] of the bridge; $\mathbf{C}_b$, the damping matrix of the bridge derived from the assumption of linear relation between the mass and stiffness matrices, which can be expressed as Eq. (8) [23]:

$$\mathbf{C}_b = p\mathbf{M}_b + q\mathbf{K}_b \tag{8}$$

where

$$p = \frac{2\omega_1\omega_2(h_1\omega_2 - h_2\omega_1)}{\omega_2^2 - \omega_1^2} \tag{9}$$

$$q = \frac{2(h_2\omega_2 - h_1\omega_1)}{\omega_2^2 - \omega_1^2} \tag{10}$$

In Eqs. (9) and (10), ω_1 and ω_2 are the first and second natural circular frequencies of the bridge system, respectively; h_1 and h_2, damping constants according to two modes of vibration with natural circular frequencies of ω_1 and ω_2. In this study, h_1 and h_2 are assumed to have the same values due to the difficulty involved in estimating the second damping constant h_2 [23].

The displacement vector of the bridge is written generally in terms of the normal coordinate as shown in Eq. (11).

$$\mathbf{D} = \sum_{j=1}^{n} \phi_j a_j = \mathbf{\Phi a} \tag{11}$$

where, $\mathbf{\Phi}$ and $\mathbf{a}$ are the modal matrix and the generalized displacement vector of the bridge, respectively.

The displacement of the bridge $w(t, x_{mu})$ can be obtained using a combination of the displacement and distribution vectors as shown in Eq. (12).

$$w(t, x_{mu}) = \boldsymbol{\Psi}_{mu}{}^{T}\mathbf{D} \tag{12}$$

where, $\boldsymbol{\Psi}_{mu}$ is the distribution vector delivering wheel loads through a plate element to each node of the element, and represented as Eq.(13).

$$\boldsymbol{\Psi}_{mu} = \left[0;\cdots;0;\Psi_{k,mu}(t);\Psi_{k+1,mu}(t);\Psi_{k+2,mu}(t);\Psi_{k+3,mu}(t);\cdots;0\right] \tag{13}$$

The final formulation of the governing differential equations for the bridge-vehicle interaction system is obtained from the relationships in Eqs. (1)-(13):

$$\begin{aligned}&\overline{\mathbf{M}}_b\ddot{\mathbf{a}} + \overline{\mathbf{C}}_b\dot{\mathbf{a}} + \overline{\mathbf{K}}_b\mathbf{a} + \boldsymbol{\Phi}^T\sum_{m=1}^{3}\sum_{u=1}^{2}\boldsymbol{\Psi}_{mu}\left(C_{vm2u}\boldsymbol{\Psi}_{mu}{}^{T}\boldsymbol{\Phi}\dot{\mathbf{a}} + K_{vm2u}\boldsymbol{\Psi}_{mu}{}^{T}\boldsymbol{\Phi}\mathbf{a}\right)\\&-\boldsymbol{\Phi}^T\sum_{m=1}^{3}\sum_{u=1}^{2}\boldsymbol{\Psi}_{mu}\left(C_{vm2u}\dot{R}_{m2u} + K_{vm2u}R_{m2u}\right) = \boldsymbol{\Phi}^T\sum_{m=1}^{3}\sum_{u=1}^{2}\boldsymbol{\Psi}_{mu}\left(W_{mu} + C_{vm2u}\dot{Z}_{rmu} + K_{vm2u}Z_{rmu}\right)\end{aligned} \tag{14}$$

$$m_{v11}\ddot{Z}_{11} + \sum_{m=1}^{2}\sum_{u=1}^{2}\left(C_{vm1u}\dot{R}_{m1u} + K_{vm1u}R_{m1u}\right) = 0 \tag{15}$$

$$-\sum_{u=1}^{2}\left(C_{v12u}\boldsymbol{\Psi}_{1u}{}^{T}\boldsymbol{\Phi}\dot{\mathbf{a}} + K_{v12u}\boldsymbol{\Psi}_{1u}{}^{T}\boldsymbol{\Phi}\mathbf{a}\right) + m_{v12}\ddot{Z}_{12} - \sum_{k=1}^{2}\sum_{u=1}^{2}(-1)^k\left(C_{v1ku}\dot{R}_{1ku} + K_{v1ku}R_{1ku}\right) = -\sum_{u=1}^{2}\left(C_{v12u}\dot{Z}_{r1u} + K_{v12u}Z_{r1u}\right) \tag{16}$$

$$\begin{aligned}&-\sum_{m=2}^{3}\sum_{u=1}^{2}\left(C_{vm2u}\boldsymbol{\Psi}_{mu}{}^{T}\boldsymbol{\Phi}\dot{\mathbf{a}} + K_{vm2u}\boldsymbol{\Psi}_{mu}{}^{T}\boldsymbol{\Phi}\mathbf{a}\right)\\&+ m_{v22}\ddot{Z}_{22} + \sum_{m=2}^{3}\sum_{k=1}^{2}\sum_{u=1}^{2}(-1)^k\left(C_{vmku}\dot{R}_{mku} + K_{vmku}R_{mku}\right) = -\sum_{m=2}^{3}\sum_{u=1}^{2}\left(C_{vm2u}\dot{Z}_{rmu} + K_{vm2u}Z_{rmu}\right)\end{aligned} \tag{17}$$

$$J_{x11}\ddot{\theta}_{x11} - \sum_{m=1}^{2}\sum_{u=1}^{2}(-1)^u\lambda_{y1}\left(C_{vm1u}\dot{R}_{m1u} + K_{vm1u}R_{m1u}\right) = 0 \tag{18}$$

$$\begin{aligned}&\sum_{u=1}^{2}(-1)^u\lambda_{y2}\left(C_{v12u}\boldsymbol{\Psi}_{1u}{}^{T}\boldsymbol{\Phi}\dot{\mathbf{a}} + K_{v12u}\boldsymbol{\Psi}_{1u}{}^{T}\boldsymbol{\Phi}\mathbf{a}\right)\\&+ J_{x12}\ddot{\theta}_{x12} - \sum_{k=1}^{2}\sum_{u=1}^{2}(-1)^k(-1)^u\lambda_{y2}\left(C_{v1ku}\dot{R}_{1ku} + K_{v1ku}R_{1ku}\right) = \sum_{u=1}^{2}(-1)^u\lambda_{y2}\left(C_{v12u}\dot{Z}_{r1u} + K_{v12u}Z_{r1u}\right)\end{aligned} \tag{19}$$

$$\begin{aligned}&\sum_{m=2}^{3}\sum_{u=1}^{2}(-1)^u\lambda_{y3}\left(C_{vm2u}\boldsymbol{\Psi}_{mu}{}^{T}\boldsymbol{\Phi}\dot{\mathbf{a}} + K_{vm2u}\boldsymbol{\Psi}_{mu}{}^{T}\boldsymbol{\Phi}\mathbf{a}\right) + J_{x22}\ddot{\theta}_{x22}\\&-\sum_{m=2}^{3}\sum_{k=1}^{2}\sum_{u=1}^{2}(-1)^k(-1)^u\lambda_{y3}\left(C_{vmku}\dot{R}_{mku} + K_{vmku}R_{mku}\right) = \sum_{m=2}^{3}\sum_{u=1}^{2}(-1)^u\lambda_{y3}\left(C_{vm2u}\dot{Z}_{rmu} + K_{vm2u}Z_{rmu}\right)\end{aligned} \tag{20}$$

$$J_{y11}\ddot{\theta}_{y11} - \sum_{m=1}^{2}\sum_{u=1}^{2}(-1)^m\lambda_{xm}\left(C_{vm1u}\dot{R}_{m1u} + K_{vm1u}R_{m1u}\right) = 0 \tag{21}$$

$$
\begin{aligned}
&-\sum_{m=2}^{3}\sum_{u=1}^{2}(-1)^m \lambda_{x3}\left(C_{vm2u}\boldsymbol{\Psi}_{mu}{}^T\boldsymbol{\Phi}\dot{\mathbf{a}}+K_{vm2u}\boldsymbol{\Psi}_{mu}{}^T\boldsymbol{\Phi}\mathbf{a}\right)\\
&+J_{y22}\ddot{\theta}_{y22}+\sum_{m=2}^{3}\sum_{u=1}^{2}(-1)^m \lambda_{x3}\left(C_{vm2u}\dot{R}_{m2u}+K_{vm2u}R_{m2u}\right)=-\sum_{m=2}^{3}\sum_{u=1}^{2}(-1)^m \lambda_{x3}\left(C_{vm2u}\dot{Z}_{rmu}+K_{vm2u}Z_{rmu}\right)
\end{aligned}
\tag{22}
$$

where, $\overline{\mathbf{M}}_b$, $\overline{\mathbf{C}}_b$ and $\overline{\mathbf{K}}_b$ in Eq. (14) refer to normalized mass, damping and stiffness matrices, respectively: $\overline{\mathbf{M}}_b=\boldsymbol{\Phi}^T\mathbf{M}_b\boldsymbol{\Phi}$; $\overline{\mathbf{C}}_b=\boldsymbol{\Phi}^T\mathbf{C}_b\boldsymbol{\Phi}$; $\overline{\mathbf{K}}_b=\boldsymbol{\Phi}^T\mathbf{K}_b\boldsymbol{\Phi}$.

The dynamic wheel loads at each tire of the vehicle are estimated based on the following formula:

$$
P_{mu}(t)=W_{mu}+C_{vm2u}\left[\dot{R}_{m2u}-\left(\boldsymbol{\Psi}_{mu}^T\,\boldsymbol{\Phi}\,\dot{\mathbf{a}}-\dot{Z}_{rmu}\right)\right]+K_{vm2u}\left[R_{m2u}-\left(\boldsymbol{\Psi}_{mu}^T\,\boldsymbol{\Phi}\,\mathbf{a}-Z_{rmu}\right)\right];\quad \mathrm{m}=1,2,3 \tag{23}
$$

The equations of the bridge-vehicle interaction are represented as following a matrix formation by combining Eqs. (14)-(23):

$$
\mathbf{M}_s\ddot{\mathbf{W}}+\mathbf{C}_s\dot{\mathbf{W}}+\mathbf{K}_s\mathbf{W}=\mathbf{F}_s \tag{24}
$$

where, $\mathbf{M}_s$, $\mathbf{C}_s$ and $\mathbf{K}_s$ indicate the mass, damping and stiffness matrices of the bridge-vehicle interaction system, respectively. The $\ddot{\mathbf{W}}$, $\dot{\mathbf{W}}$, $\mathbf{W}$ and $\mathbf{F}_s$ respectively refer to the acceleration, velocity, displacement and force vectors of the system. Details concerning the system matrices are described in the Appendix section.

By eliminating elements of the column and row related to θ_{y22} in the system matrices and replacing 1/4 of Eq. (7) to 1/2, the Eq. (24) can be applied to the bridge-vehicle interaction problem exposed to the two-axle vehicle (7DOF vehicle). Neglecting the matrices and variables related to the bridge response in Eq. (24) allows for the dynamic response analysis for a vehicle operating on the rigid surface.

The dynamic equation for the vehicle-bridge interaction is a non-stationary dynamic problem since the coefficient matrices of the equations vary according to the vehicle position. Thus, the simultaneous differential equations involved in the bridge-vehicle interaction system are solved using Newmark β as a direct integration method [19].

4. Numerical examples

4.1. Numerical models

The bridge studied in this paper is a steel plate girder bridge with a span measuring 40.4m in length. It is composed of three girders and reinforced concrete (RC) decks. Figure 3 shows the general layout and FE model

of the bridge and details of the bridge model are summarized in Table 1.

Mode shapes from the eigen value analysis are shown in Fig. 4 with natural frequencies taken from analysis and experiment. The first natural frequencies for bending and torsion obtained through analysis represent a reasonable match for those obtained through experimental results. It assists the validity of bridge modeling for the dynamic response analysis.

Table 2 shows details of the vehicle models. The spring constants and damping coefficients of the two-axle vehicle are estimated in DIVINE (Dynamic Interaction Vehicle-INfrastructure Experiment) project developed by the OECD [21]. Part of the project was coordinated by the TNO (Road-Vehicles Research Institute of Netherlands Organization for Applied Scientific Research) working under the auspices of the DIVINE joint research program [20]. In field tests, vehicle speeds were measured up to 64.96km/hr, 75.68km/hr and 82.73km/hr respectively with sample rates of 100Hz used during the experiments.

For the three-axle vehicle, the spring constants and damping coefficients of suspensions in Table 2 are measured during the on-site test at Umeda entrance bridge in Osaka, Japan [16, 22, 27]. For tires, on the other hand, the test has not been performed; meaning empirically assumed values of the truck manufacturer are used in the analysis. The vehicle speeds during the experiment were measured as 14.0 ~ 17.3km/hr, 21.7 ~ 23.9km/hr and 30.0 ~ 31.5km/hr. The sample rates were 100Hz during the experiments.

Measured roadway profiles used in analyses are shown in Fig. 5(a) [20, 21] and Fig. 5(b) [16, 22, 27]. The profiles are designated as P1-profile and P2-profile respectively in this paper. The roadway profiles were sampled every 0.05m and the state of the roadway profiles can be categorized as very good (Class A) according to ISO estimate [28] based on the vehicle ride comfort compared to the power spectral density (PSD) curves (see Fig. 6).

Under analysis, the vehicle speeds recorded are then used to compare analytical and experimental results. A time step of 0.001 sec for bridge and vehicle models and β of 0.25 are used to obtain a stable and accurate solution. The solution can be obtained within the relative margin of error of less than 0.001.

4.2. Verification of numerical results

4.2.1. Dynamic wheel loads of two-axle vehicle

To verify the validity of the analytical dynamic wheel loads of the two-axle cargo truck running on the rigid roadway, time histories of wheel loads, the dynamic load coefficient (DLC) [20, 21] and dominant frequencies of wheel loads for each tire are compared to the field test data. The DLC is defined as the ratio of the root mean square (RMS) dynamic wheel loads against the mean wheel load where the RMS dynamic wheel load represents the standard deviation of the probability distribution. The DLC is hence the wheel load coefficient of variation. Since the DLC value has a limited role in validating the model, the cumulative distribution function is also adopted as a function to analyze and validate the model. The measured dynamic wheel load of the two-axle

vehicle running on the P1-profile is taken from the DIVINE project [20, 21].

Figures 7 and 8 show, respectively, time histories and PSD curves of dynamic wheel loads of the two-axle vehicle at v=82.73km/hr, and positive correlation is observed between analytical and experimental results.

To assess the validity of the analytical dynamic wheel loads quantitatively, cumulative distributions, DLC values and dominant frequencies of the wheel loads are compared with experimental ones. Cumulative distributions of the dynamic wheel load in Fig. 7 are shown in Fig. 9, and the DLC values and dominant frequencies are summarized in Table 3. The correlation between the analysis and experiment shown in Fig. 9 and Table 3 demonstrates that the model is capable of simulating the dynamic wheel loads within an error margin of under 10 percent on average. One thing worth noting in Table 3 is that dominant frequencies of the dynamic wheel loads vary according to speed. One of the reasons for such dominant frequency variation may be the propensity for the dominant space frequency of the roadway profile, which can resonant with a vehicle system, to change in accordance to the vehicle speed.

4.2.2. Acceleration responses of three-axle vehicle

The experiment for the three-axle vehicle was carried out as a part of a field test for the Umeda entrance bridge located on the Hanshin Expressway in Osaka, Japan [16, 22, 27]. The acceleration responses in relation to bounce and axle-hop motions are taken from accelerometers equipped on the vehicle body and each axle. The roadway profile measured under the path of the three-axle vehicle is the P2-profile (see Fig. 5(b)).

Acceleration responses of the bounce and the axle-hop motion of the vehicle are shown in Fig. 10. It is clear that the quality of the correlation between the experimental and analytical results is considered quite acceptable for the bounce motion. Figure 11 shows a positive correlation of PSD curves for the bounce motion comparing experiment and analysis. On the other hand, poorly assumed spring constant and damping coefficient related to tires leads the axle-hop motion which somewhat differs from the experimental result. The dominant frequencies of the bounce and axle-hop motion of the three-axle vehicle are summarized in Table 4.

4.2.3. Bridge responses

The Figure 12 shows typical strain responses taken from analysis and field tests at the span centre of the main bridge girders due to the passage of the three-axle vehicle with P2-profile on the bridge. The PSD curves of the strain responses are shown in Fig. 13. G1 and G2 in the Figs. 12 and 13 indicate the external and internal girders, respectively (see Fig. 3(a)). The trends, maximum amplitudes and overall responses match quite well.

The dynamic increment factor (DIF) [29] is chosen as a parameter for the quantitative investigation of bridge responses. The DIF is defined as the ratio of absolute maximal difference between the dynamic and static responses to the maximum static response during one major period of the dynamic response including the maximum static response (see Fig. 14) [29]. The ΔY in Fig. 14 is expressed as $\Delta Y = |Y_{\mathrm{dynamic}} - Y_{\mathrm{static}}|_{\max}$. DIF values

of the bridge are summarized in Table 5, which also shows a positive correlation between experiment and analysis despite the poor assumption of tire-related properties.

4.2.4. Summary

The summarized results for the relationship between experiment and analysis are plotted in Fig. 15, which illustrates the ratio of analytical to experimental results. It is observed that the analytic DLC values of the two-axle vehicle wheel loads are distributed between 88% and 110% of the experimental ones. The dominant frequencies of wheel loads of the two-axle vehicle taken from analysis represent between 84% and 110% of the experimental results. On the other hand, the analytical frequencies of the bounce motion and the axle-hop motion of the three-axle vehicle range from 80% to 120% and 60% to 145% of the experimental results, respectively. The damping coefficient and spring constant for each tire of the three-axle vehicle used in analysis are not measured but taken as empirically assumed values, and the ratios between the analytical and experimental results of the three-axle vehicle are thus scattered more widely than those of the two-axle vehicle. For DIF values of the bridge, analytical results are distributed between 93% and 105% of the experimental ones.

The field test data indicates that the analytical method is accurate for predicting the dynamic wheel load and response of highway bridges induced by moving vehicles.

5. Conclusions

In this study, the simultaneous differential equations of motion to simulate the dynamic responses of the bridge-vehicle interaction system are derived using the Lagrange equation of motion from Hamilton's principle, and FE method for modal analysis is adopted. The major conclusions that can be drawn from the analysis and experiment are as follows:

1. Analytical dynamic wheel loads provide good results when the properties of the vehicle are well estimated or tested. The analytical DLC values and dominant frequencies for wheel loads of the two-axle vehicle are scattered within 88% ~ 110% and 84% ~ 110% of the experimental results, respectively.
2. For the three-axle vehicle, the dominant frequencies of the bounce motion correlate positively with experimental results –representing 80% ~ 120% of these latter. On the other hand, for the axle-hop motion, a less accurate correlation between the analytical and experimental results than those of bounce motion is observed, namely 60% ~ 145% of the experimental results, because of the difference of the accuracy in assuming the spring constant of tires.
3. The analytical DIF values of the bridge display a positive correlation with the experimental results despite the tire stiffness being poorly estimated: i.e. the values are distributed at 93% and 105% of the experimental

results. It encourages the use of assumed properties for tires during the simulation, where the analysis is focused on the dynamic responses of medium span bridges with similar frequency characteristics to the bounce motion of vehicles.

4. The field test data indicates that analytical method to be accurate for predicting the dynamic wheel load and response of highway bridges induced by moving vehicles.

Appendix A

The Eq. (24) can be expressed as follows:

$$\begin{bmatrix} \overline{\mathbf{M}}_b & 0 \\ Symm. & \mathbf{M}_v \end{bmatrix} \begin{Bmatrix} \ddot{\mathbf{a}} \\ \ddot{\Delta} \end{Bmatrix} + \begin{bmatrix} \overline{\mathbf{C}}_b^{\,*} & \overline{\mathbf{C}}_{bv} \\ Symm. & \mathbf{C}_v \end{bmatrix} \begin{Bmatrix} \dot{\mathbf{a}} \\ \dot{\Delta} \end{Bmatrix} + \begin{bmatrix} \overline{\mathbf{K}}_b^{\,*} & \overline{\mathbf{K}}_{bv} \\ Symm. & \mathbf{K}_v \end{bmatrix} \begin{Bmatrix} \mathbf{a} \\ \Delta \end{Bmatrix} = \begin{Bmatrix} \overline{\mathbf{f}}_b \\ \mathbf{f}_v \end{Bmatrix} \tag{A1}$$

where,

$$\overline{\mathbf{M}}_b = \begin{bmatrix} M_{b1} & \cdots & 0 \\ \vdots & \ddots & \vdots \\ Symm. & \cdots & M_{bn} \end{bmatrix} \tag{A2}$$

$$\mathbf{M}_v = \begin{bmatrix} m_{v11} & & & & & & & \\ & m_{v12} & & & & & & \\ & & m_{v22} & & & 0 & & \\ & & & J_{x11} & & & & \\ & & & & J_{x12} & & & \\ & & Symm. & & & J_{y22} & & \\ & & & & & & J_{y11} & \\ & & & & & & & J_{x22} \end{bmatrix} \tag{A3}$$

$$\overline{\mathbf{C}}_b^{\,*} = \begin{bmatrix} \overline{C}_{b1} + \Phi_1^{\,T} \sum_{m=1}^{3} \sum_{u=1}^{2} \Psi_{mu} C_{vm2u} \Psi_{mu}^{\,T} \Phi_1 & & \mathbf{0} \\ & \ddots & \\ Symm. & & \overline{C}_{bn} + \Phi_n^{\,T} \sum_{m=1}^{3} \sum_{u=1}^{2} \Psi_{mu} C_{vm2u} \Psi_{mu}^{\,T} \Phi_n \end{bmatrix} \tag{A4}$$

$$\overline{\mathbf{C}}_{bv} = \begin{bmatrix} 0 & C_{bv12} & C_{bv13} & 0 & C_{bv15} & C_{bv16} & 0 & C_{bv18} \\ \vdots & \vdots & \vdots & \vdots & \vdots & \vdots & \vdots & \vdots \\ 0 & C_{bvn2} & C_{bvn3} & 0 & C_{bvn5} & C_{bvn6} & 0 & C_{bvn8} \end{bmatrix} \tag{A5}$$

$$C_{bvj2} = -\sum_{u=1}^{2} C_{v12u} \boldsymbol{\Psi}_{1u}^{\,T} \boldsymbol{\Phi}_j \,; \quad C_{bvj3} = -\sum_{m=2}^{3} \sum_{u=1}^{2} C_{vmnu} \boldsymbol{\Psi}_{mu}^{\,T} \boldsymbol{\Phi}_j \,; \quad C_{bvj5} = \sum_{u=1}^{2} (-1)^u \lambda_{y2} C_{v12u} \boldsymbol{\Psi}_{1u}^{\,T} \boldsymbol{\Phi}_j \,;$$

$$C_{bvj6} = \sum_{m=2}^{3} \sum_{u=1}^{2} (-1)^u \lambda_{y3} C_{vm2u} \boldsymbol{\Psi}_{mu}^{\,T} \boldsymbol{\Phi}_j \,; \quad C_{bvj8} = -\sum_{m=2}^{3} \sum_{u=1}^{2} (-1)^m \lambda_{x3} C_{vm2u} \boldsymbol{\Psi}_{mu}^{\,T} \boldsymbol{\Phi}_j \,; \; j=1\sim n.$$

$$\mathbf{C}_v = \begin{bmatrix} C_v^{11} & C_v^{12} \\ C_v^{21} & C_v^{22} \end{bmatrix} \tag{A6}$$

$$\mathbf{C}_v^{11} = \begin{bmatrix} \sum_{m=1}^{2}\sum_{u=1}^{2} C_{vm1u} & -\sum_{u=1}^{2} C_{v11u} & -\sum_{u=1}^{2} C_{v21u} & -\sum_{m=1}^{2}\sum_{u=1}^{2} (-1)^u \lambda_{y1} C_{vm1u} \\ & \sum_{k=1}^{2}\sum_{u=1}^{2} C_{v1ku} & 0 & \sum_{u=1}^{2} (-1)^u \lambda_{y1} C_{v11u} \\ & & \sum_{u=1}^{2}(C_{v21u} + \sum_{m=2}^{3} C_{vm2u}) & \sum_{u=1}^{2} (-1)^u \lambda_{y1} C_{v21u} \\ & \textit{Symm.} & & \sum_{m=1}^{2}\sum_{u=1}^{2} {\lambda_{y1}}^2 C_{vm1u} \end{bmatrix}$$

$$\mathbf{C}_v^{12} = \begin{bmatrix} \sum_{u=1}^{2} (-1)^u \lambda_{y2} C_{v11u} & \sum_{u=1}^{2} (-1)^u \lambda_{y3} C_{v21u} & -\sum_{m=1}^{2}\sum_{u=1}^{2} (-1)^m \lambda_{xm} C_{vm1u} & 0 \\ -\sum_{k=1}^{2}\sum_{u=1}^{2} (-1)^u \lambda_{y2} C_{v1ku} & 0 & -\sum_{u=1}^{2} \lambda_{x1} C_{v11u} & 0 \\ 0 & -\sum_{u=1}^{2} (-1)^u \lambda_{y3}(C_{v21u} + \sum_{m=2}^{3} C_{vm2u}) & \sum_{u=1}^{2} \lambda_{x2} C_{v21u} & \sum_{m=2}^{3}\sum_{u=1}^{2} (-1)^m \lambda_{x3} C_{vm2u} \\ -\sum_{u=1}^{2} \lambda_{y1}\lambda_{y2} C_{v11u} & -\sum_{u=1}^{2} \lambda_{y1}\lambda_{y3} C_{v21u} & \sum_{m=1}^{2}\sum_{u=1}^{2} (-1)^m (-1)^u \lambda_{xm}\lambda_{y1} C_{vm1u} & 0 \end{bmatrix}$$

$$\mathbf{C}_v^{22} = \begin{bmatrix} \sum_{k=1}^{2}\sum_{u=1}^{2} {\lambda_{y2}}^2 C_{v1ku} & 0 & \sum_{u=1}^{2} (-1)^u \lambda_{x1}\lambda_{y2} C_{v11u} & 0 \\ & \sum_{u=1}^{2} {\lambda_{y3}}^2 (C_{v21u} + \sum_{m=2}^{3} C_{vm2u}) & -\sum_{u=1}^{2} (-1)^u \lambda_{y3}\lambda_{x2} C_{v21u} & -\sum_{m=2}^{3}\sum_{u=1}^{2} (-1)^m (-1)^u \lambda_{x3}\lambda_{y3} C_{vm2u} \\ & & \sum_{m=1}^{2}\sum_{u=1}^{2} {\lambda_{xm}}^2 C_{vm1u} & 0 \\ & \textit{Symm.} & & \sum_{m=2}^{3}\sum_{u=1}^{2} {\lambda_{x3}}^2 C_{vm2u} \end{bmatrix}$$

$$\mathbf{C}_v^{21} = \mathbf{C}_v^{12}$$

A similar procedure can be employed to derive each element in $\overline{\mathbf{K}}_b^{\,*}$, $\overline{\mathbf{K}}_{bv}$ and $\mathbf{K}_v$ matrices.

The displacement and force vectors shown in Eq. (A1) are defined as;

$$\{\mathbf{a};\ \ \boldsymbol{\Delta}\} = \{a_1;\ \ \cdots;\ \ a_n;\ \ Z_{11};\ \ Z_{12};\ \ Z_{22};\ \ \theta_{x11};\ \ \theta_{x12};\ \ \theta_{x22};\ \ \theta_{y11};\ \ \theta_{y22}\} \tag{A7}$$

$$\bar{\mathbf{f}}_b = \boldsymbol{\Phi}^T \left\{ \sum_{m=1}^{3}\sum_{u=1}^{2} \Psi_{mu} \left(W_{mu} + K_{vm2u} Z_{rmu} + C_{vm2u} \dot{Z}_{rmu} \right) \right\} \tag{A8}$$

$$\begin{aligned} \mathbf{f}_v = \Big\{ & 0; -\sum_{u=1}^{2} (K_{v21u} Z_{r1u} + C_{v21u} \dot{Z}_{r1u}); -\sum_{m=2}^{3}\sum_{u=1}^{2} (K_{vm2u} Z_{rmu} + C_{vm2u} \dot{Z}_{rmu}); 0; \sum_{u=1}^{2} (-1)^u \lambda_{y2} (K_{v12u} Z_{r1u} + C_{v12u} \dot{Z}_{r1u}); \\ & \sum_{m=2}^{3}\sum_{u=1}^{2} (-1)^u \lambda_{y3} (K_{vm2u} Z_{rmu} + C_{vm2u} \dot{Z}_{rmu}); 0; -\sum_{m=2}^{3}\sum_{u=1}^{2} (-1)^m \lambda_{x3} (K_{vm2u} Z_{rmu} + C_{vm2u} \dot{Z}_{rmu}) \Big\} \end{aligned} \tag{A9}$$

References

[1] Timoshenko SP. History of strength of materials. Dover; 1982. p.173-181.

[2] Cantieni R. Dynamic behavior of highway bridges under the passage of heavy vehicles. EMPA Report No. 220; 1992.

[3] The AASHO road test: Report 4-Bridge Research, Special Report 61D: National Academy of Science-National Research Council; 1962.

[4] Walker WH, Veletsos AS. Response of simple-span highway bridges to moving vehicles. Bulletin 486: Univ. of Illinois, Engineering Experiment Station, Urbana IL; 1966.

[5] Nieto-Ramirez JA, Veletsos AS. Response of three-span continuous highway bridges to moving vehicles. Bulletin 489: Univ. of Illinois, Engineering Experiment Station, Urbana IL; 1966.

[6] Hwang ES, Nowak AS. Simulation of dynamic load for bridges. J Struct Eng ASCE 1991; 117: 1413-1434.

[7] Hutton SG, Cheung YK. Dynamic response of single span highway bridges. Earthq Eng Struct Dyn 1979; 7: 543-553.

[8] Billing JR. Dynamic loading and testing of bridges in Ontario. Can J Civ Eng CSCE 1984; 11: 833-843.

[9] Honda H, Kobori T, Yamada Y. Dynamic factor of highway steel girder bridges. IABSE Proceedings 1986; P-98: 57-75.

[10] Inbahathan MJ, Wieland M. Bridge vibrations due to vehicle moving over rough surface. J Struct Eng ASCE 1987; 113(9): 1994-2008.

[11] Kou JW, DeWolf JT. Vibrational behavior of continuous span highway bridge-Influencing variables. J of Struct Eng ASCE 1997; 123(3): 333-344.

[12] Biggs JM. Introduction to structural dynamics. McGraw-Hill; 1982. p.315-327.

[13] Green MF, Cebon D. Dynamic interaction between heavy vehicles and highway bridges. Comput Struct 1997; 62(2); 253-264.

[14] Pesterev AV, Bergman LA. Response of elastic continuum carrying moving linear oscillator. J Eng Mech ASCE 1997; 123(8): 878-884.

[15] Yang YB, Lin BH. Vehicle –bridge interaction analysis by dynamic condensation method. J Struct Eng ASCE 1995; 121(11): 1636-1643.

[16] Kawatani M, Kim CW. Effects of gap at expansion joint on traffic-induced vibration of highway bridge. In: Proceedings of Developments in short and medium span bridge engineering'98, Calgary, Canada, 1998. p.285-294.

[17] Mulcathy NL. Bridge response with tractor-trailer vehicle loading. Earthquake Eng Struct Dyn 1983; 11: 649-665.

[18] Huang D, Wang TL. Vibration of highway steel bridges with longitudinal grades. Comput Struct 1998; 69(2); 235-245.

[19] Newmark NM. A method of computation for structural dynamics. J Eng Mech Div ASCE 1970; 96:

593-620.

[20] Hoogvelt RBJ, Ruijs PAJ. OECD-IR6 DIVINE Element 4. Computer simulation of heavy vehicle dynamic wheel loads. TNO Report 97.OR.016.1/H/PR, TNO, Delft, The Netherlands; 1997.

[21] Technical Report, DSTI/DOT/RTR/IR6(98)1FINAL, OECD; 1998.

[22] Kim CW, Kawatani M. A comparative study on dynamic wheel loads of multi-axle vehicle and bridge responses. In: Proceedings of DETC'01 ASME 2001 Design Engineering Technical Conference and Computers and Information in Engineering Conference, Pittsburgh, USA, 2001. (CD-ROM)

[23] Agabein ME. The effect of various damping assumptions on the dynamic response of structures. Bulletin of international institute of seismology and earthquake engineering. Building Research Institute of Japan 1971; 8: 217-236.

[24] Bathe KJ. Finite element procedures in engineering analysis. Prentice-Hall; 1982.

[25] Guyan RJ. Reduction of stiffness and mass matrices. AIAA J 1965; 3(2): 380.

[26] Hurty W. C. and Rubinstein, M. F. Dynamics of structures. Prentice-Hall; 1960. p.90-103.

[27] Technical report-Inspections on Umeda entrance bridge structures. Hanshin Expressway Public Corporation (HEPC), 1992. (in Japanese)

[28] ISO 8608. Mechanical Vibration – Road Surface Profiles – Reporting of Measured Data. ISO; 1995.

[29] Kawatani M, Nishiyama S, Yamada Y. Dynamic response analysis of highway bridges under moving vehicle. Technical Report of the Osaka Univ. 1993; 43(2137): 109-118.

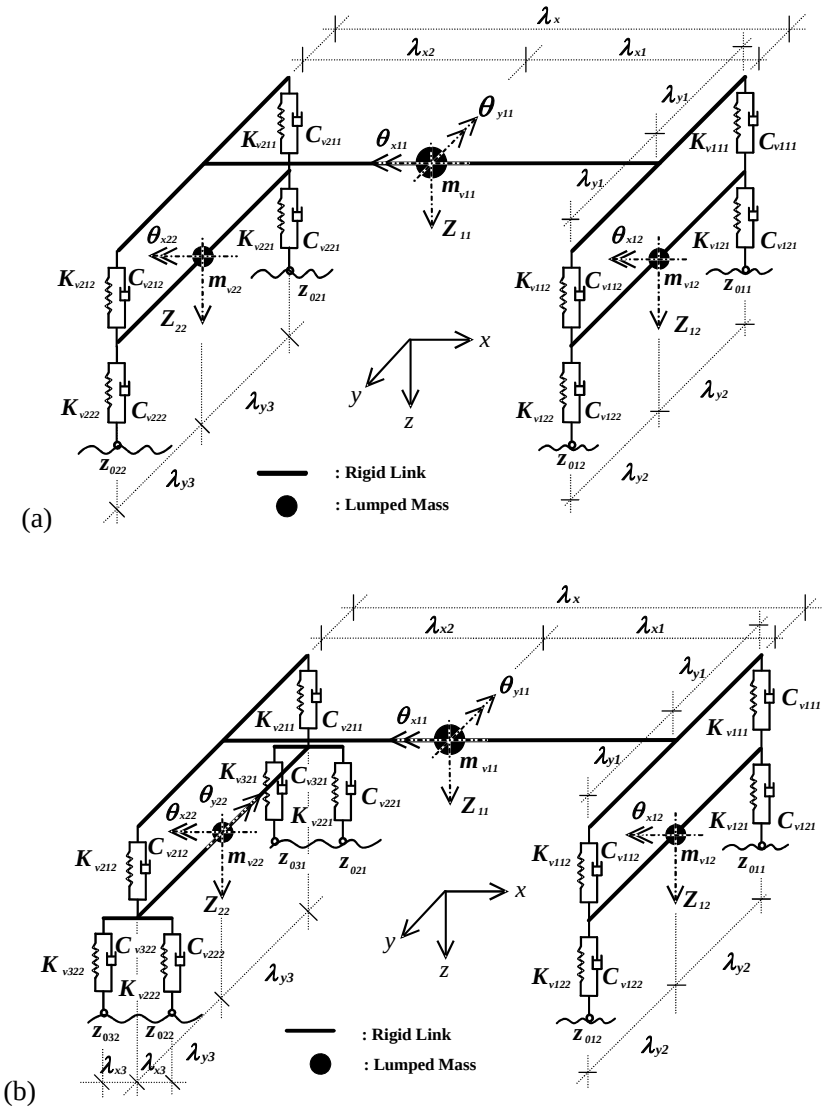

Fig. 1. Idealized heavy trucks. (a) Two-axle vehicle with seven-degrees-of-freedom, (b) Three-axle vehicle with eight-degrees-of-freedom.

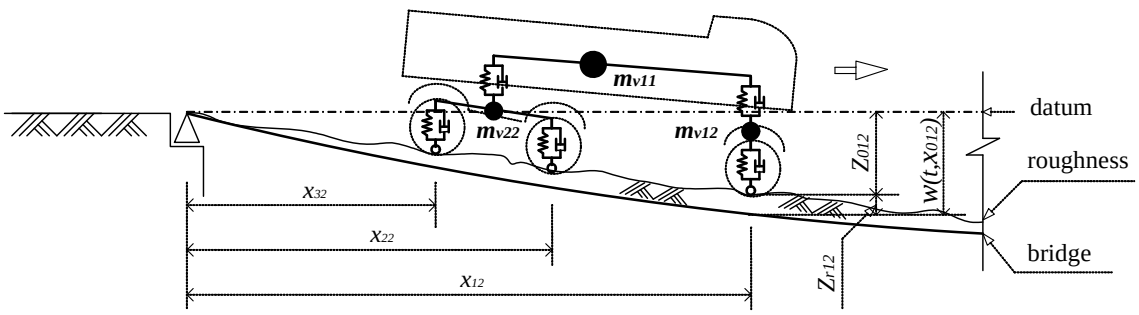

Fig. 2. Bridge-vehicle interaction system.

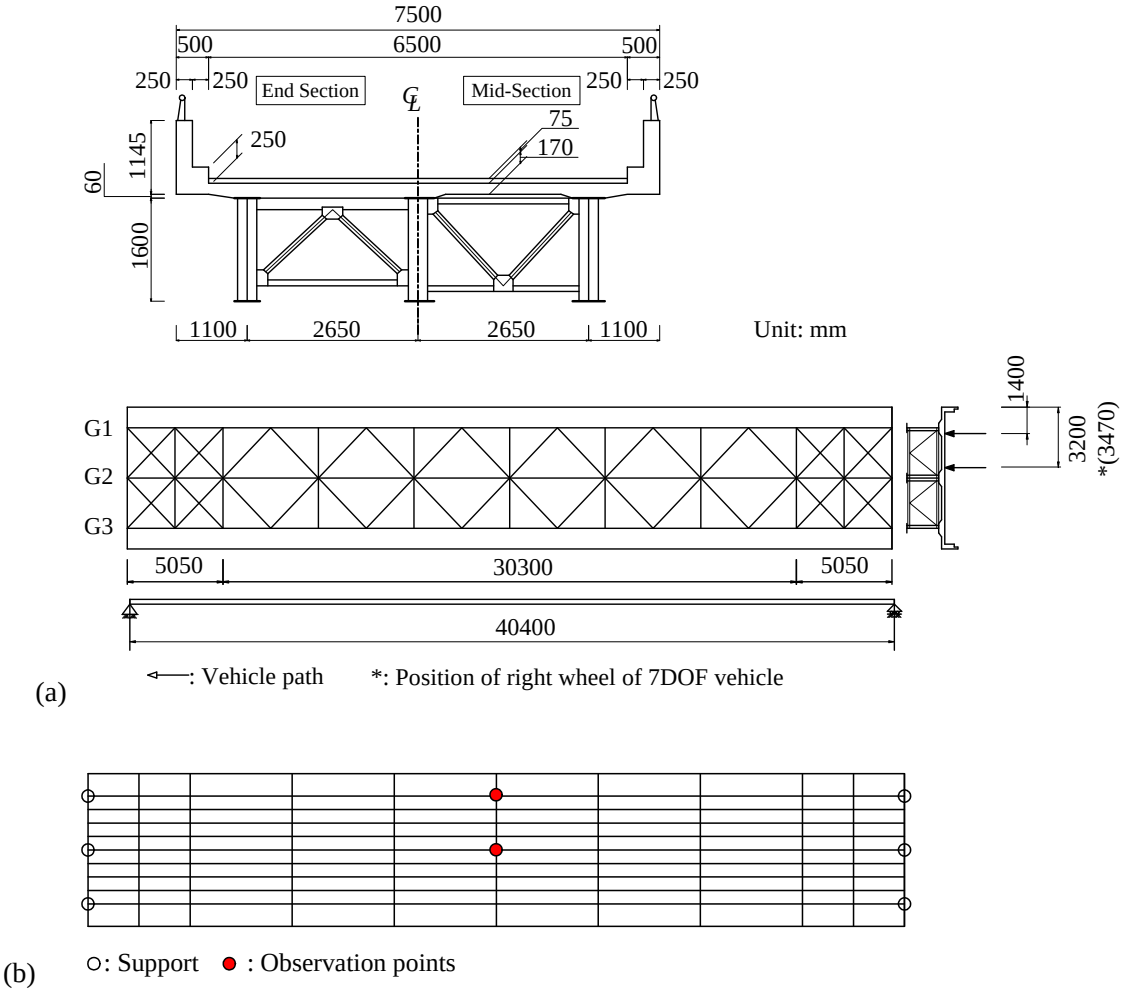

Fig. 3. Steel plate girder bridge. (a) General layout, (b) FE model.

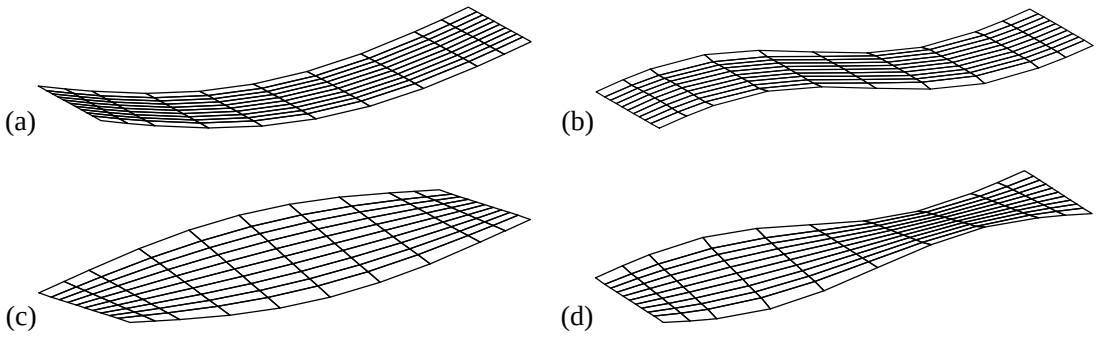

Fig. 4. Mode shapes and fundamental natural frequencies of steel girder bridge. (a) First bending mode (Analysis: 2.32Hz, Experiment: 2.33Hz), (b) Second bending mode (Analysis: 8.79Hz), (c) First torsion mode (Analysis: 3.56Hz, Experiment: 3.86Hz), (d) Second torsion mode (Analysis: 9.68Hz).

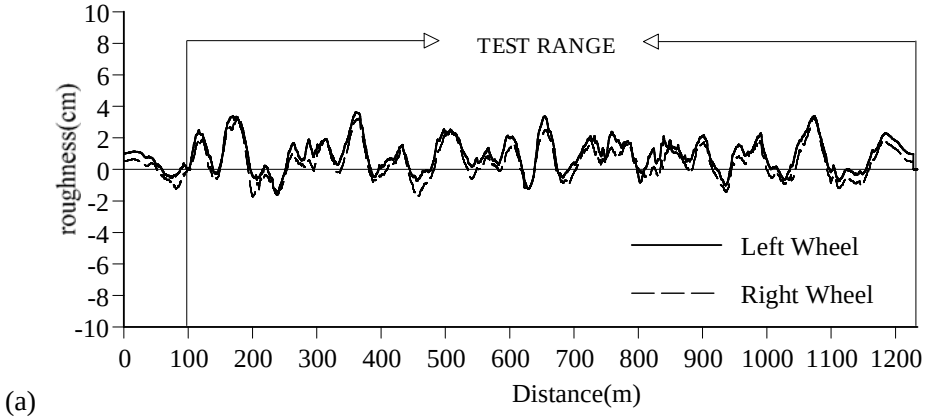

(a)

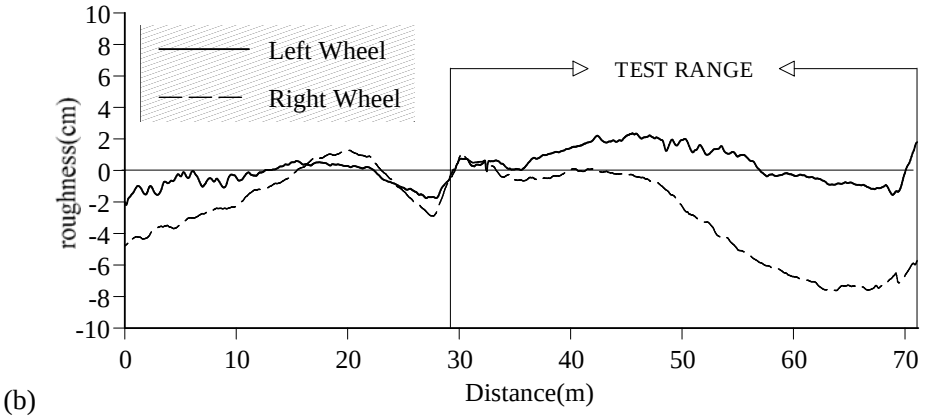

(b)

Fig. 5. Measured roadway profiles. (a) Smooth Canadian Road (P1-Profile), (b) Umeda Entrance Road (P2-Profile).

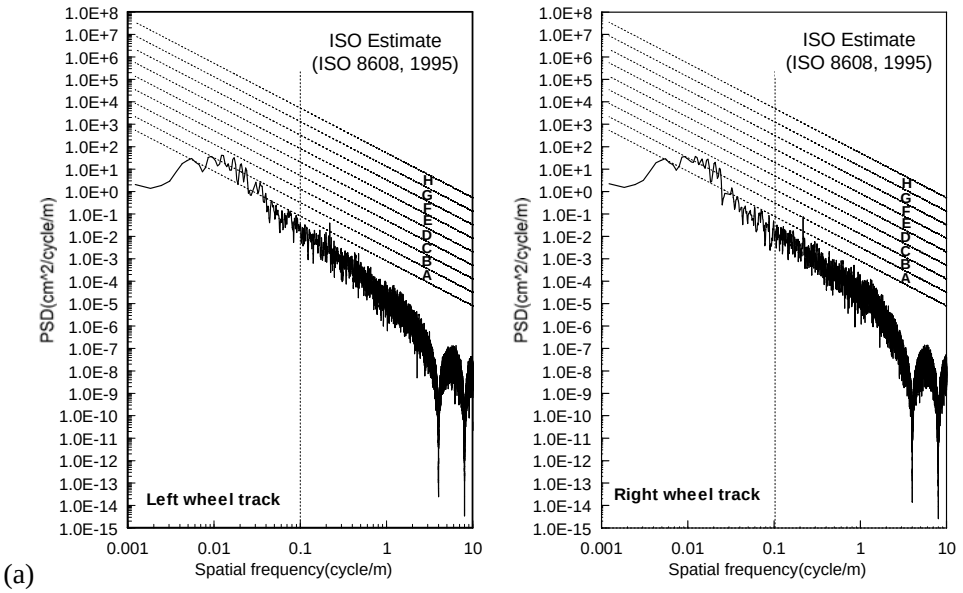

(a)

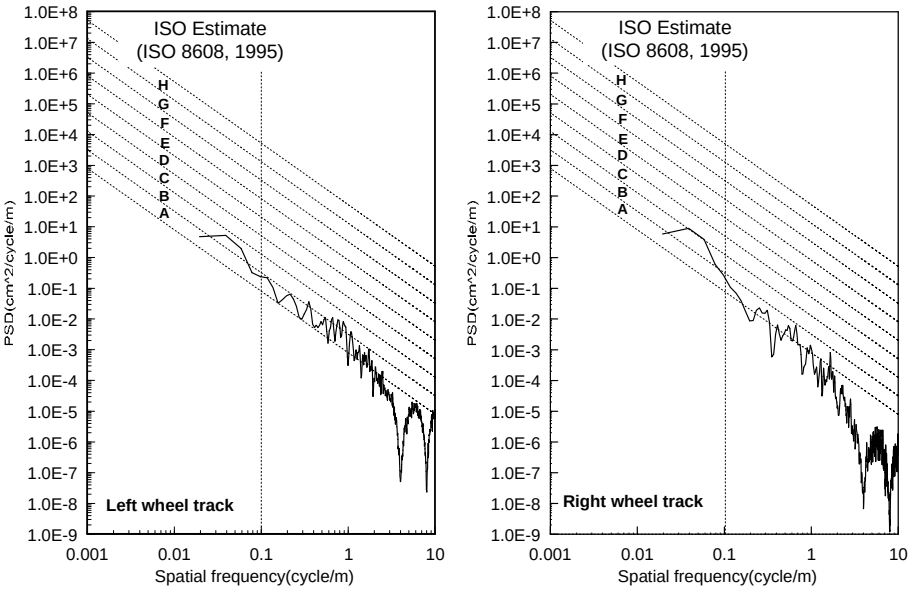

(b)

Fig. 6. PSD curves of measured roadway profiles. (a) P1-profile, (b) P2-profile.

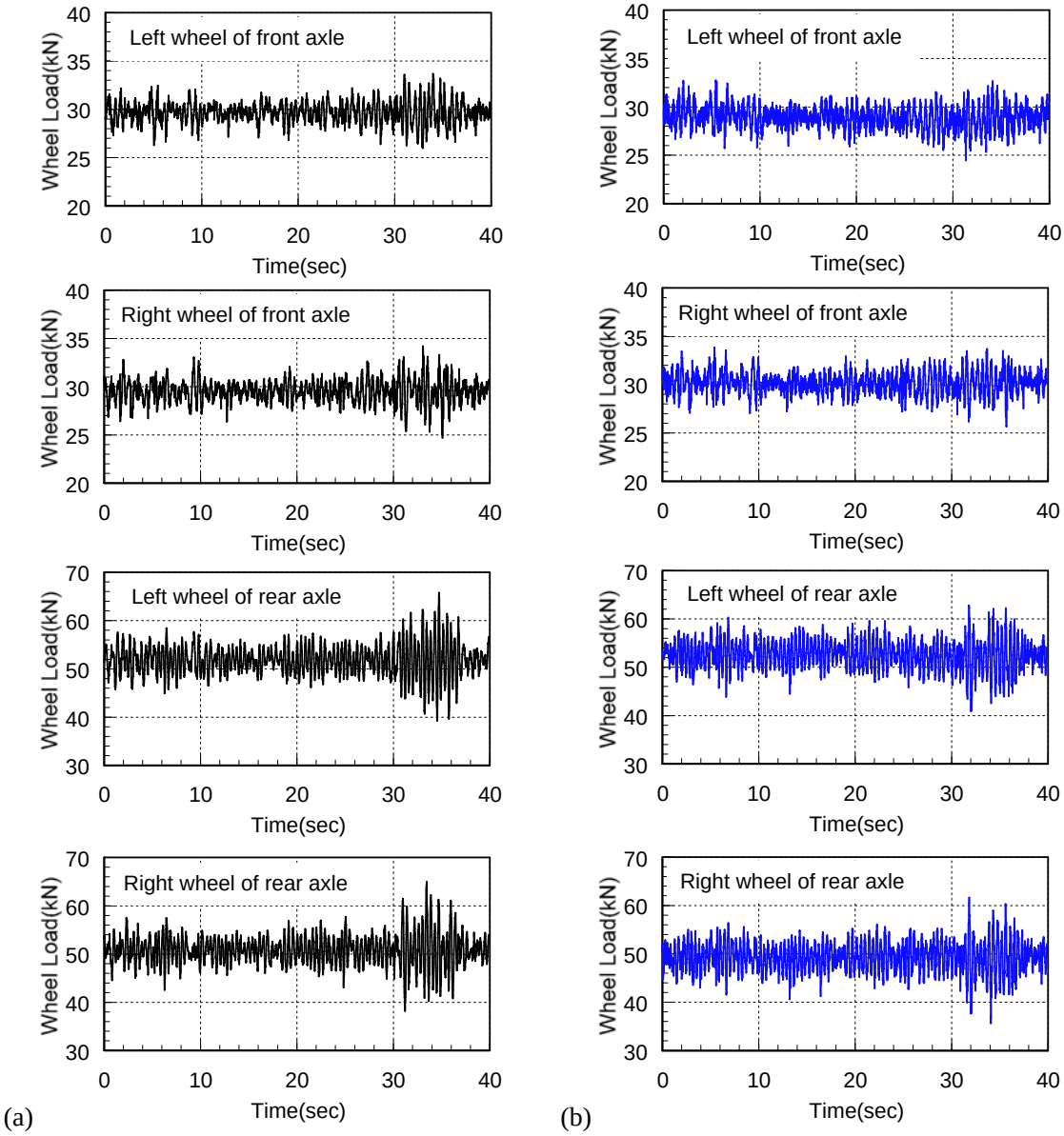

Fig. 7. Dynamic wheel loads of two-axle vehicle (v=82.73km/hr). (a) Analysis, (b) Field-test.

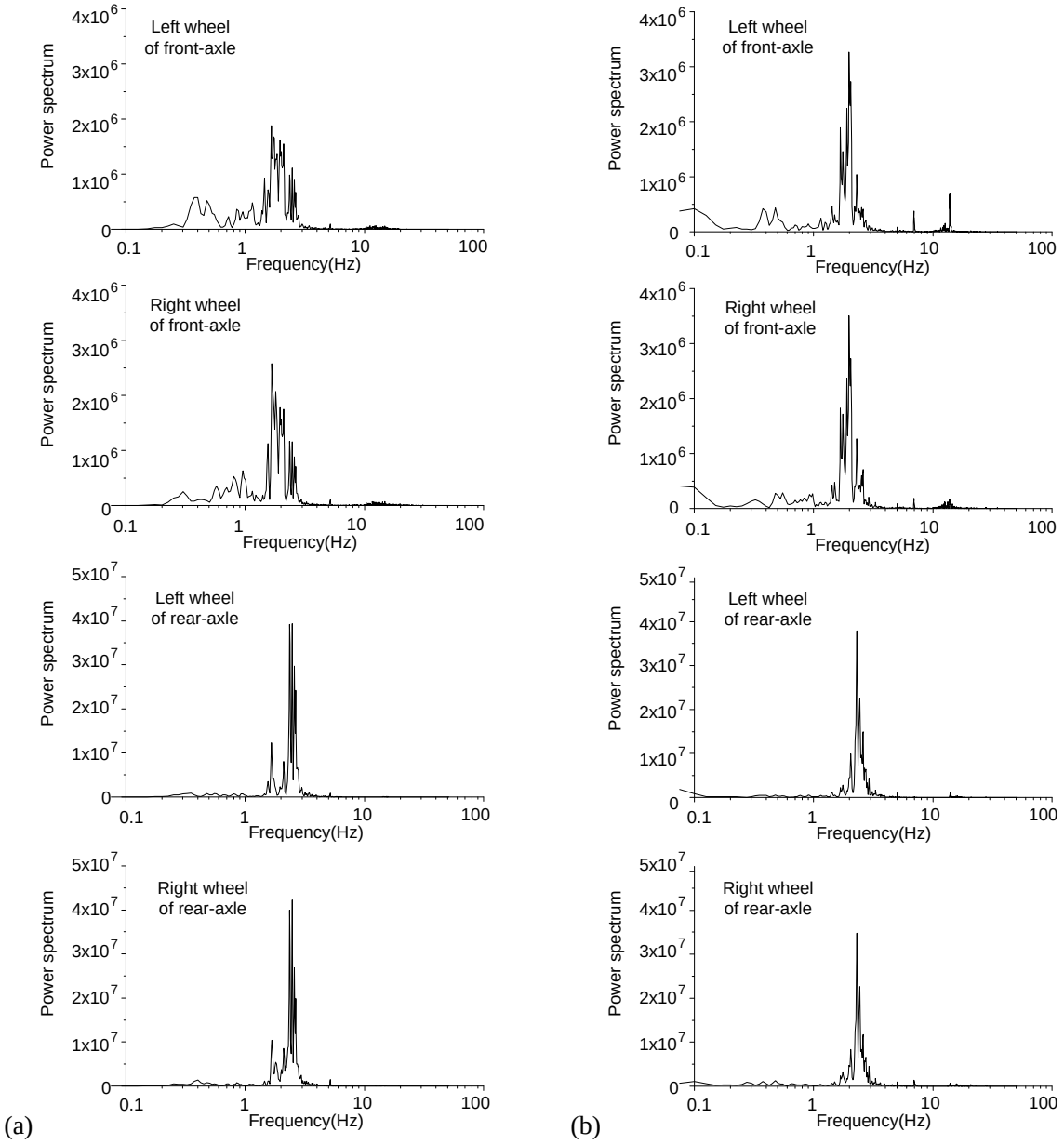

Fig. 8. PSD curves of dynamic wheel loads in Fig. 7 (v=82.73km/hr). (a) Analysis, (b) Field-test.

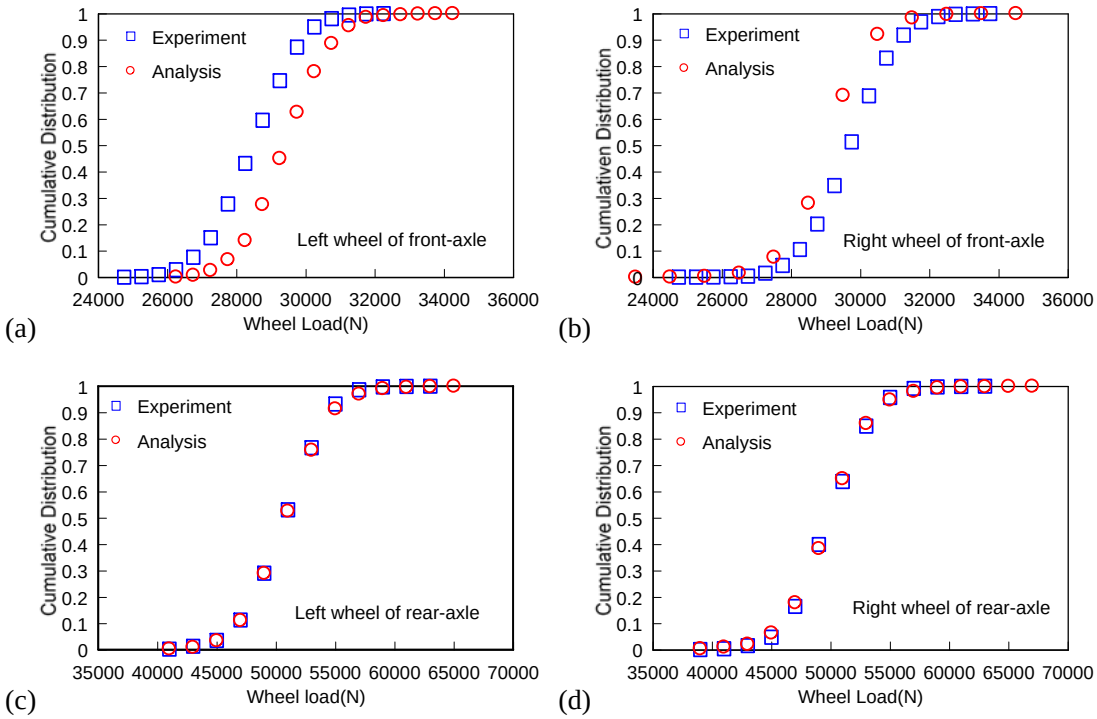

Fig. 9. Cumulative distributions of dynamic wheel loads of two-axle vehicle in Fig. 7 (v=82.73km/hr). (a) Left wheel of front-axle, (b) Right wheel of front-axle, (c) Left wheel of rear-axle, (d) Right wheel of rear-axle.

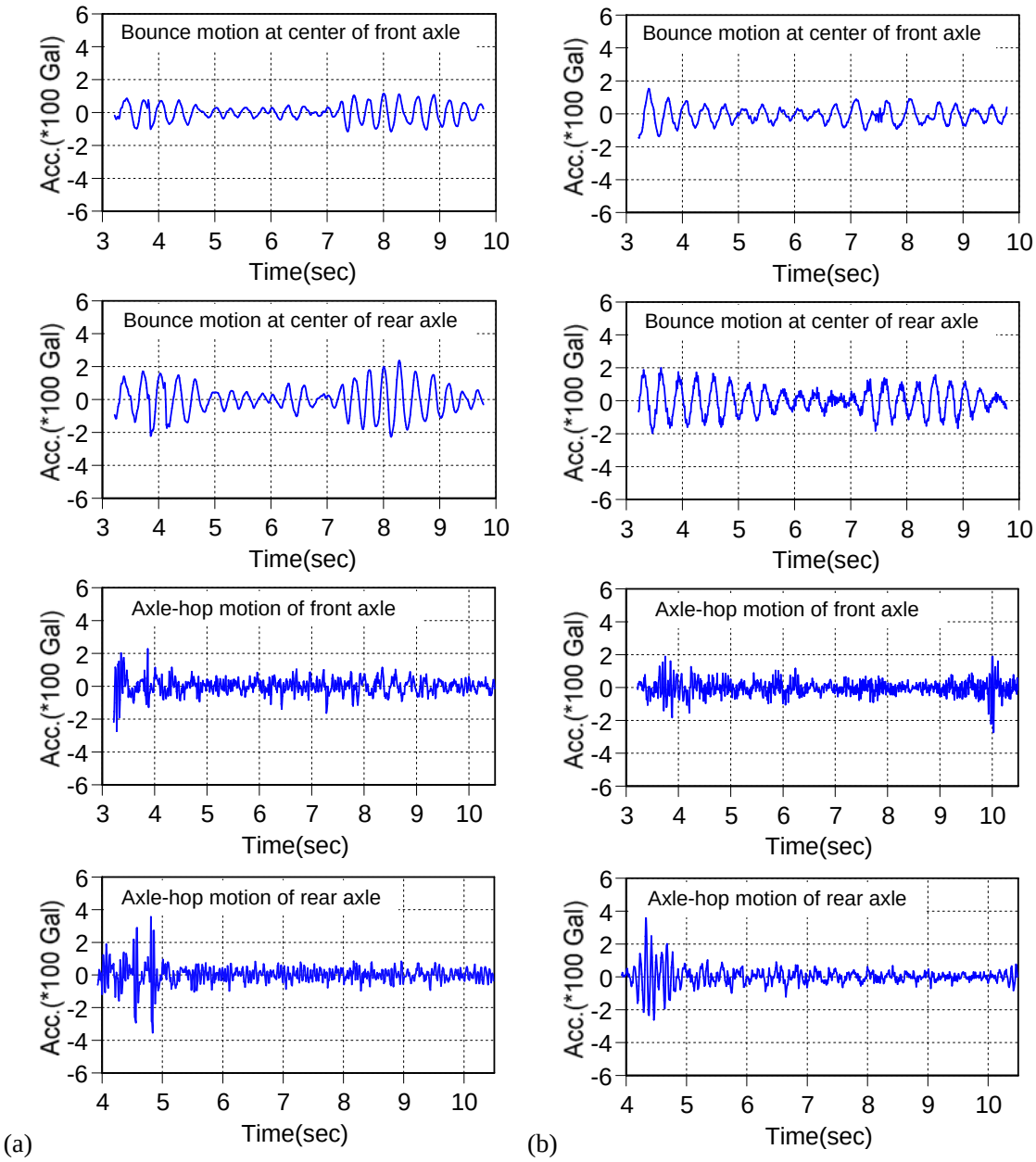

Fig. 10. Acceleration time histories of three-axle vehicle (v=16.8km/hr). (a) Analysis, (b) Field-test.

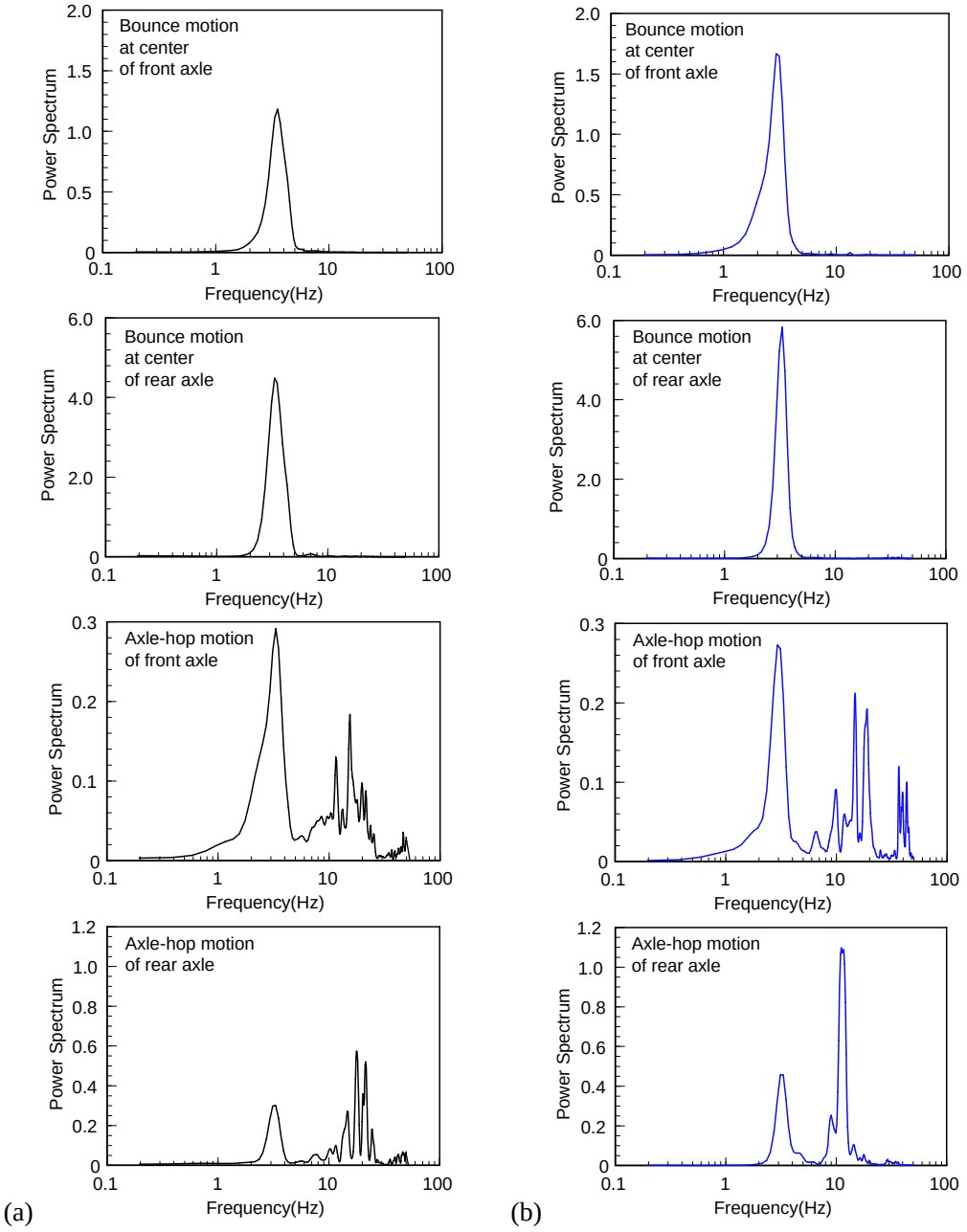

Fig. 11. PSD curves of accelerations in Fig. 10 (v=16.8km/hr). (a) Analysis, (b) Field-test.

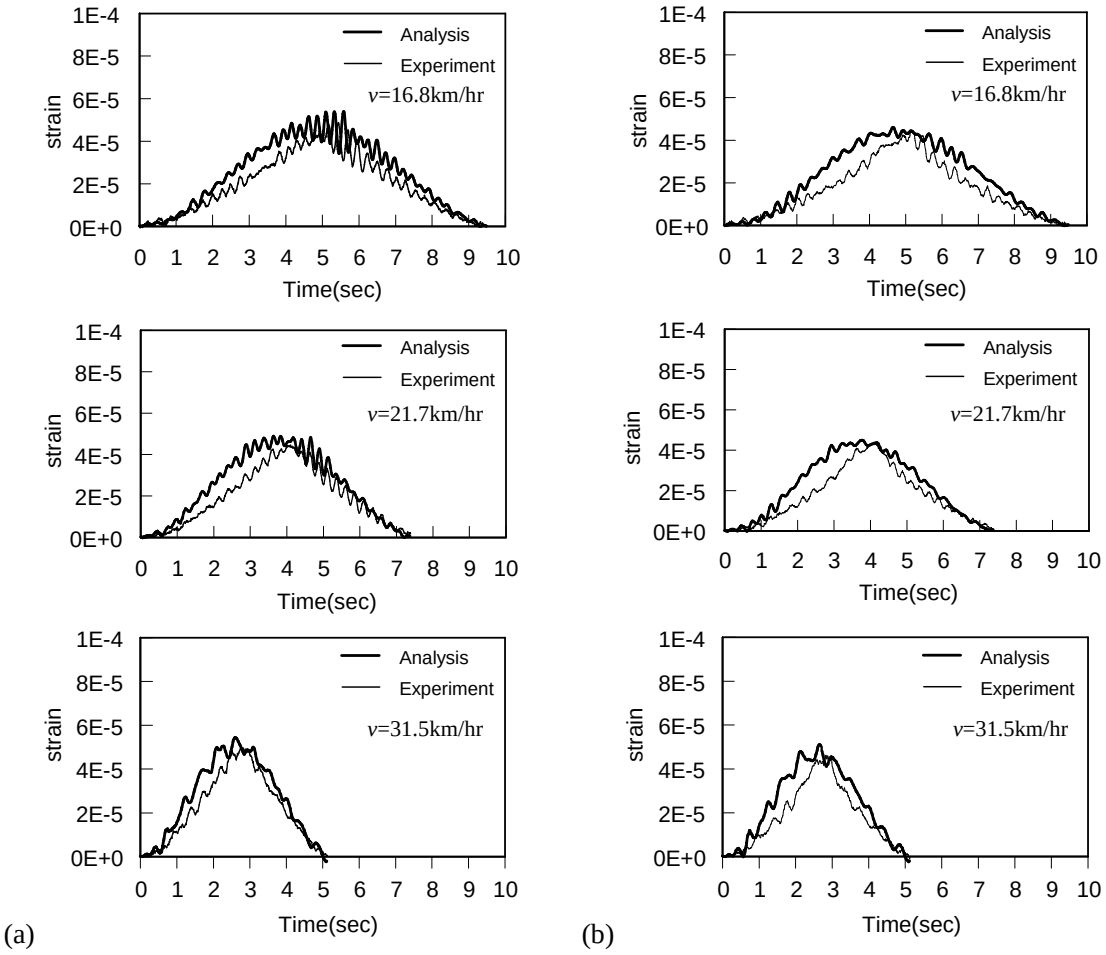

Fig. 12. Strain responses of bridge due to three-axle vehicle running on P2-profile. (a) External girder G1 at span centre, (b) Internal girder G2 at span centre.

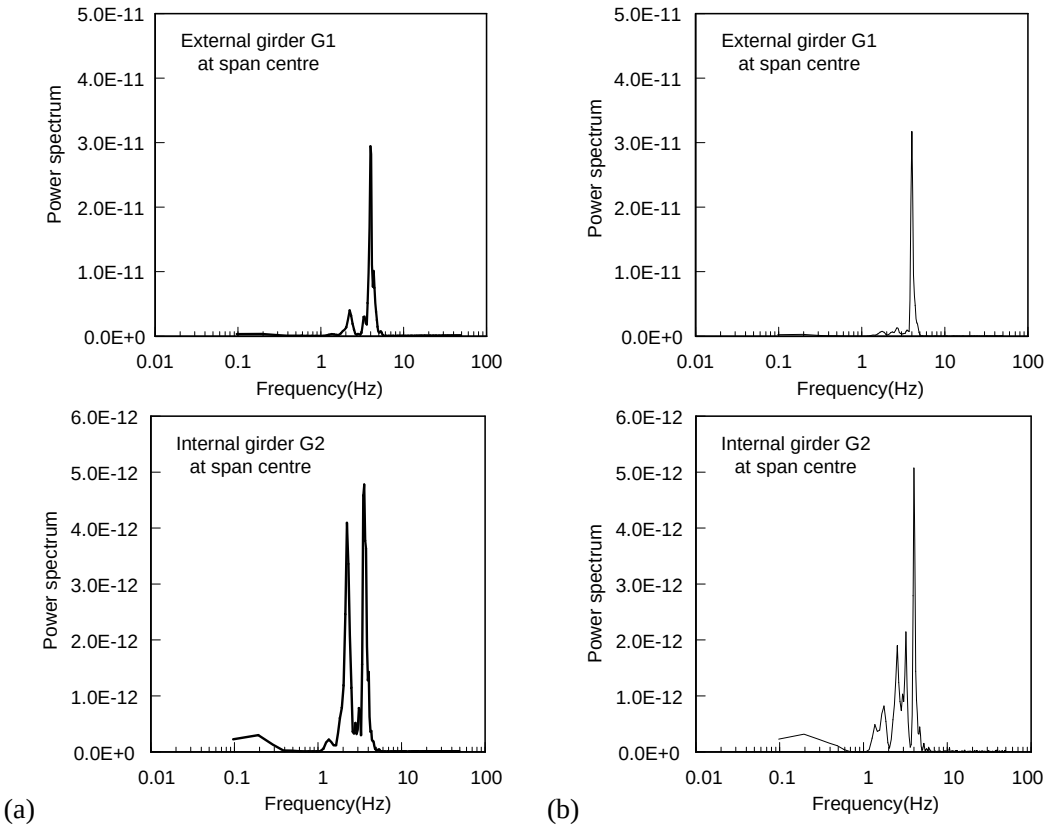

Fig. 13. PSD curves of bridge responses in Fig. 12 (v=21.7km/hr). (a) Analysis, (b) Field-test.

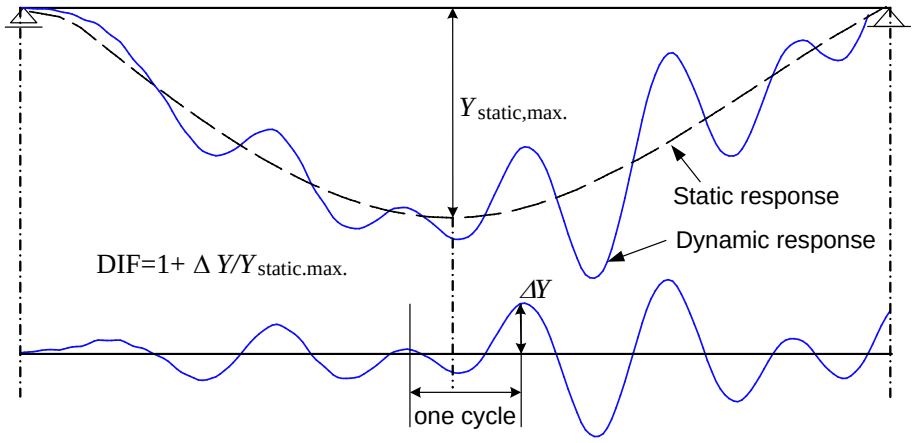

Fig. 14. Definition of DIF.

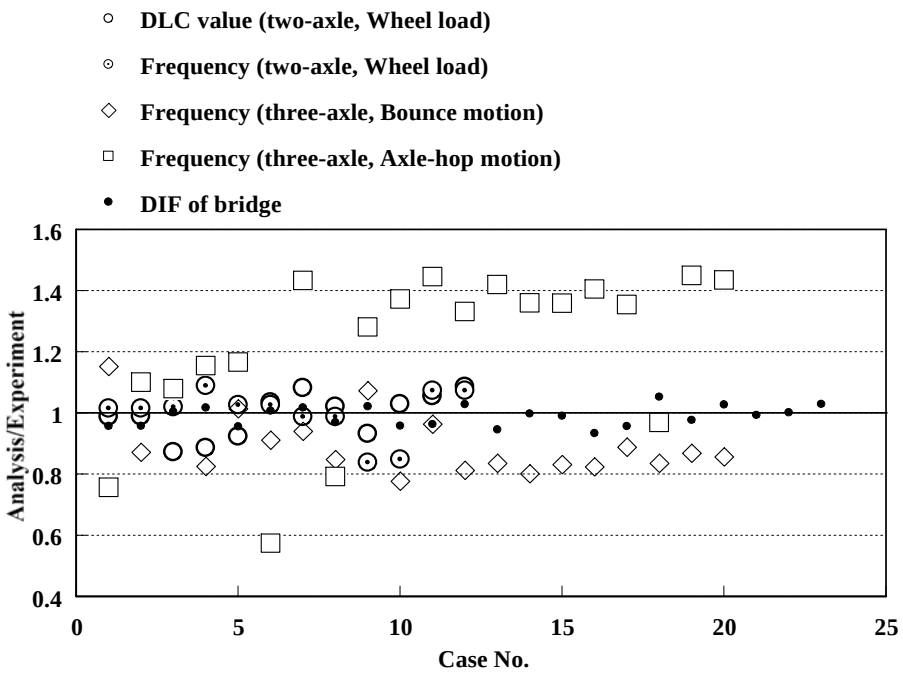

Fig. 15. Ratio of analytical and experimental results.

Table 1

Properties of steel bridge

Mass per unit length(kg/m)		7,550
Section area of girders(m^2)		0.1420
Moment of inertia(m^4)		0.2120
Torsional constant(m^4)		0.0548
Damping constant(for 1st and 2nd modes)		0.0253
Fundamental frequency (Experiment, Hz)	1-st (Bending)	2.33
	2-nd (Torsion)	3.86

Table 2

Properties of vehicles

Parameter		Two-axle vehicle	Three-axle vehicle
Geometry (m)	Tread	2.07	1.80
	Distance between front and rear axle	6.20	3.99
	Distance of tandem axle	-	1.20
	Distance between front axle and center of gravity	3.94	2.99
Mass (kg)	Sprung mass including payload	14,790	18,500
	Steer axle un-sprung mass	650	500
	Drive axle un-sprung mass	1,070	1,450
Spring constant of suspension (kN/m)	Front leaf spring	475	1,577
	Rear leaf spring	1,820	4,724
Spring constant of tire (kN/m)	Front tire	1,390	3,146
	Rear tire	1,170	4,724
Damping coefficient of suspension (kN·s/m)	Front left	7.810	11.200
	Front right	8.065	11.200
	Rear left	3.324	33.420
	Rear right	1.649	33.420
Damping coefficient of tire (kN·s/m)	Front tire	-	13.300
	Rear tire	-	10.000

Table 3

DLC values and dominant frequencies of dynamic wheel loads of two-axle vehicle

Vehicle speed (km/hr)	Wheel	DLC		Dominant frequency (Hz)	
		Experiment	Analysis	Experiment	Analysis
64.96	Front left	0.0309	0.0328	1.93	1.96
	Front right	0.0319	0.0337	1.93	1.96
	Rear left	0.0444	0.0511	2.53	2.58
	Rear right	0.0471	0.0531	2.53	2.58
75.68	Front left	0.0342	0.0394	1.88	1.93
	Front right	0.0357	0.0371	1.88	1.93
	Rear left	0.0579	0.0572	2.46	2.43
	Rear right	0.0582	0.0609	2.46	2.43
82.73	Front left	0.0384	0.0399	1.98	1.66
	Front right	0.0397	0.0377	1.98	1.66
	Rear left	0.0632	0.0598	2.31	2.48
	Rear right	0.0649	0.0601	2.31	2.48

Table 4

Dominant frequencies of three-axle vehicle

Roadway condition	Vehicle speed (km/hr)	Position	Bounce motion		Axle-hop motion	
			Experiment	Analysis	Experiment	Analysis
Case1	16.8	front	3.47	4.00	22.90	17.33
		rear	4.15	4.00	14.11	20.40
	21.7	front	3.59	3.13	17.39	19.14
		rear	4.33	3.52	14.23	18.95
	31.5	front	3.28	3.52	14.11	15.23
		rear	4.21	3.52	14.17	20.20
Case2	23.2	front	4.02	3.32	17.76	20.51
		rear	4.39	3.52	14.36	19.53
	30.8	front	3.47	3.52	17.08	19.92
		rear	4.46	3.71	14.23	19.34
Case3	14.9	front	3.96	3.61	23.64	13.57
		rear	4.27	3.52	13.55	19.04
	30.0	front	3.53	3.32	14.17	20.31
		rear	4.4	3.91	13.99	18.95
Case4	17.3	front	4.15	3.52	17.02	13.48
		rear	4.21	3.52	14.91	14.45
	23.9	front	3.28	3.52	16.46	21.09
		rear	4.27	3.71	13.74	19.92
	30.9	front	4.27	3.32	14.23	19.53
		rear	4.33	3.71	13.61	19.53

Case1: P2-profile with no bump at expansion joint of entrance
Case2: P2-profile with 5mm bump (plank with 5mm thickness) at expansion joint of entrance
Case3: P2-profile with 10mm bump (plank with 10mm thickness) at expansion joint of entrance
Case4: P2-profile with 15mm bump (plank with 15mm thickness) at expansion joint of entrance

Table 5

DIF values of steel bridge

Roadway condition	Vehicle speed (km/hr)	External girder G1 (at span centre)		Internal girder G2 (at span centre)	
		Experiment	Analysis	Experiment	Analysis
Case1	16.8	1.20	1.15	1.11	1.05
	21.7	1.11	1.06	1.04	1.04
	31.5	1.09	1.09	1.10	1.09
Case2	14.0	1.13	1.15	1.21	1.06
	23.2	1.11	1.06	1.09	1.04
	30.8	1.08	1.08	1.07	1.13
Case3	14.9	1.13	1.15	1.09	1.06
	23.9	1.07	1.04	1.09	1.12
	30.0	1.10	1.12	1.06	1.06
Case4	17.3	1.20	1.15	1.07	1.07
	23.9	1.10	1.06	1.09	1.12
	30.9	1.09	1.12	-	-

Case1: P2-profile with no bump at expansion joint of entrance
Case2: P2-profile with 5mm bump (plank with 5mm thickness) at expansion joint of entrance
Case3: P2-profile with 10mm bump (plank with 10mm thickness) at expansion joint of entrance
Case4: P2-profile with 15mm bump (plank with 15mm thickness) at expansion joint of entrance